Dielectric characterization of BSA doped-PANI interlayered metal–semiconductor structures

Nursel Karaoğlan[1] · Habibe Uslu Tecimer[2] · Şemsettin Altındal[3] · Cuma Bindal[4,5]

Abstract

The measured capacitance and conductance–voltage (C&G/ω–V) data between 1 and 200 kHz of Al/(BSA-doped-PANI)/p-InP structure were examined to uncover real and imaginary components of complex permittivity ($\varepsilon^* = \varepsilon' - j\varepsilon''$), loss tangent (tanδ), complex electric modulus ($M^* = M' + jM''$), and electrical conductivity (σ). It was uncovered that dielectric constant (ε'), dielectric loss (ε''), tanδ, real and imaginary components (M' and M'') show a big dispersive behavior at low frequencies due to the oriental and the interfacial polarizations, as well as the surface states (N_{ss}) and the BSA doped-PANI interlayer. Such behavior in ε', ε'', and tanδ, behavior with frequency was also explained by Maxwell–Wagner relaxation. The values of σ are almost constant at lower-intermediate frequencies, but they start increase at high frequencies which are corresponding to the dc and ac conductivity, respectively. The values of M' and M'' are lower in the low frequency zone and they become increase with increasing frequency at accumulation region due to the short-range charge carriers mobility. Ultimately, dielectric parameters and electric modulus alteration with frequency is the consequence of surface states and relaxation phenomena.

1 Introduction

In recent years, the use of polymers with metal semiconductors (MS) has become quite common. This usage of polymers is generally shown as an interlayer between metal and semiconductor and these structures are generally named as metal-polymer-semiconductor (MPS) in the literature [1–6]. As an interlayer, the contribution of the polymers to the dielectric and electric properties has been proven many times in the previous studies [7–9]. Easy processing, lower energy

consumption, litheness and lightness are some of the superior features of organic interlayered MS structures. From this standpoint, it is possible to utilize the C–V and G/ω–V data at a wide frequency range and at appropriate voltage levels to determine the contribution of the organic polymers to the dielectric specifications of the MS structures. By the way, the obtained data from these measurements can be exploited to obtain electrical modulus (M) and electrical conductivity (σ_{ac}) electronic applications, it is also possible to study on the relaxation process by determining the electrical modulus variation with frequency [10].

Including C&G/ω–V characterizations the impedance spectroscopy provides an opportunity to determine the complex dielectric constant (ε^*) and electric modulus (M^*), loss tangent (tanδ) and σ_{ac} at various biases and frequencies [11]. Different formulations lead to identify the dielectric data of various materials [12]. Electronic and dipolar polarizations support the dielectric polarization while they actualize in a short period of time [13].

In recent years, indium phosphide (InP) has become very popular among semiconductor materials used in electronic technology. Due to its direct bandgap and high mobility properties, it has been preferred in optoelectronic and microwave applications requiring high speed and power [14–16]. InP based Schottky structures are among the essential structures for microwave circuits. On the other hand, the quality

✉ Nursel Karaoğlan
  nceran@karabuk.edu.tr

1   Department of Property Protection and Safety Division, TOBB Technical Sciences Vocational School, Karabük University, 78050 Karabük, Turkey

2   Department of Electrical-Electronic Engineering, Faculty of Engineering, Karabük University, 78050 Karabük, Turkey

3   Department of Physics, Faculty of Science, Gazi University, 06560 Ankara, Turkey

4   Department of Metallurgy and Materials Engineering, Faculty of Engineering, Sakarya University, 54187 Sakarya, Turkey

5   Sakarya University, Biomedical, Magnetic and Semi Conductive Materials Research Center (BIMAS-RC), Esentepe Campus, 54187 Sakarya, Turkey

of the metal semiconductor interface is very effective on the performance and reliability of the Schottky structures [17].

For this reason, it is important that the organic/polymer interlayer has to be uniform with controlled load carrying capacity and a suitable voltage drop that does not diverge Schottky structure from ideal behavior [18]. Doping is a very effective method to increase the conductivities of n and p types by providing extra charge carriers to organic polymers that do not have basic charge carriers. It is known that good electrical and optical results have been obtained by metal addition to the weakly conductive polymers used at M/S interface [19, 20].

Polyaniline attracts attention as a high conductivity polymer with easy doping control and color changes at different oxidation levels features. Reaction with the protonic acid can easily lead to its doping and becomes electrically conductive. In addition, the low cost, environmental stability, processability and especially conductivity properties of polyaniline and its derivatives are important reasons for choosing Polyaniline as an interlayer at MS structures. [21–23].

PANI and its derivatives has been subjected several studies on Schottky structures as an interlayer to examine the electrical and optical characterization. In these studies, basic electrical parameters (barrier height, ideality factor, rectifying ratio, etc.) have been extracted from the current–voltage and capacitance–voltage data [24, 25] Since the rectifying ratio is quite dependent on the dopant type, BSA is used as a dopant for PANI in this study. It is also important to increase the processability as well as the conductivity in the selection of the dopant [26]. PANI synthesis and electroactivity strongly depend on pH. Inorganic and organic acid to obtain a high pH in the synthesis of many widely conductive PANI are used [27–29]. Among these acids, organic acids containing large anion groups such as benzene sulfonic acid (BSA) [30], camphorsulphonic acid (CSA) [31] and dodecylbenzene sulphonic acid (DBSA) [32] have been found to increase solubility.

The main aim of this study is to fabricated the Al/(BSA-doped-PANI)/p-InP structure and were investigated the real and imaginary components of complex permittivity ($\varepsilon^* = \varepsilon' - j\varepsilon''$), loss tangent (tan$\delta$), complex electric modulus ($M^* = M' + jM''$), and electrical conductivity (σ) under proper applied biases between 1 and 200 kHz intervals by using the C–V and G/ω–V data. All these parameters show a prevalent behavior especially at lower frequency levels due to the oriental and the interfacial polarizations, the surface states (N_{ss}) and the BSA doped-PANI interlayer.

2 Experimental procedure

A schematic of the Al/BSA-PANI/p-InP structure is presented in the inset of Fig. 1. The MPS structure were fabricated on the float zone of Zn doped InP (100) wafer with having thickness, diameter and resistivity of 350 μm, 2″ and (2.77–6.95)$\times 10^{-2}$ Ω cm, respectively. The wafers were
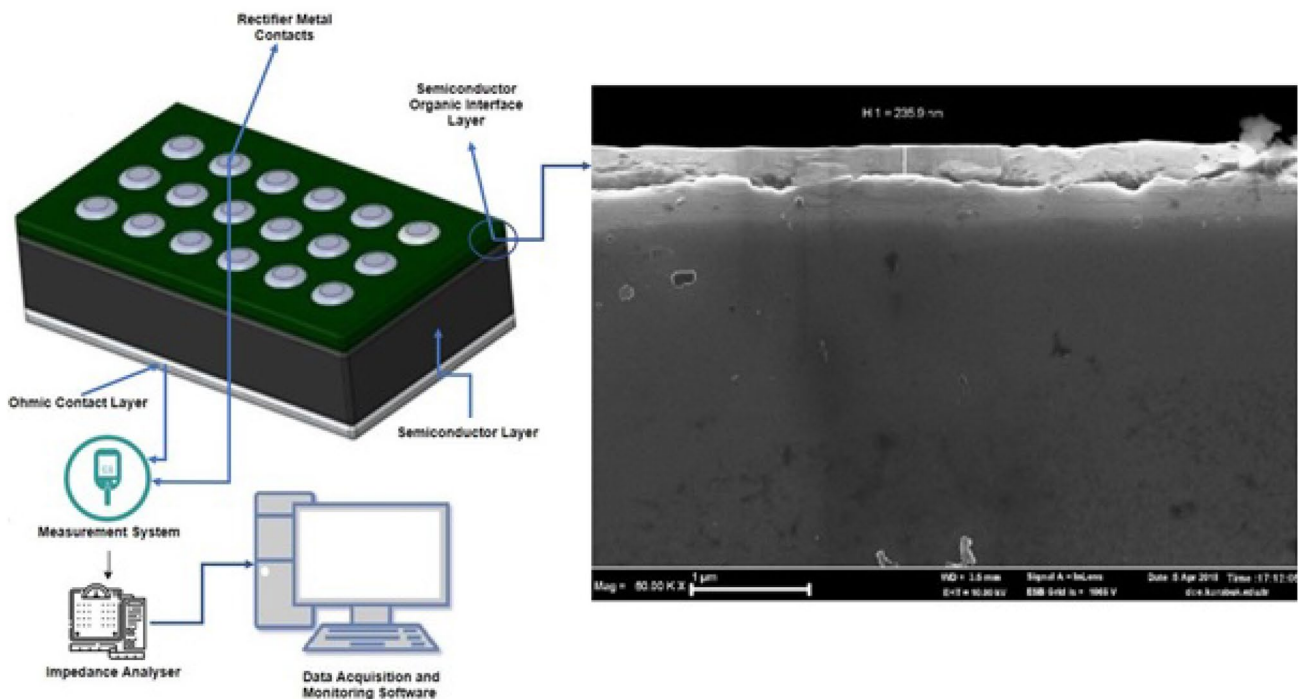

Fig. 1 Both the schematic diagram of the Al/(BSA-doped-PANI)/p-InP structures and measured impedance measurements system

initially washed with solvents such as acetone, methanol and trichlorethylene and then with purified water to remove the chemical residues. The InP wafer was then chemically washed using a dilute solution of HF: H_2O (1:20). It was rinsed with deionized water and dried in N_2 atmosphere. The chemically cleaned crystals were evaporated under the pressure of about 10^{-7} Torr in a pure aluminum (Al) metal evaporation system with a purity of % 99.999 in the thickness of 1000–1500 Å to the back mat surface to form ohmic contacts. In order perform low resistivity an ohmic contact Al/n-InP was annealed at 500 °C in the nitrogen ambient. After that PANI layer in the presence of BSA acid was synthesized by chemical oxidation method at room temperature (20 °C). Approximately %50 oxidation of the aniline monomer with ammonium peroxydisulfate a ratio of 1:1.25 was achieved and BSA-doped PANI in emeraldine salt form was obtained. To obtain an effective conductivity value, aniline monomer and BSA acid ratio is 1:1. The conductivity of the synthesized polymer was measured as 1.39 S cm^{-1} with the four-point technique. A colloidal dispersion of the PANI-BSA, whose solubility is increased by the help of SO_3 groups, was prepared having a density of 1.4 g/L in dimethlysulfoxide (DMSO). Washing and etching processes were repeated on the polished surface of the ohmic contacted InP wafer before polymer coating and rectifying contact vaporization. Then, on the front bright surface of the semiconductor crystal, PANI thin film thickness of about 200–250 nm were formed by spin coating technique. Polymer coating was carried out by dissolving the dissolved BSA-PANI solution in DMSO at dropped onto a speed of 1500 rpm into the InP surface, removing excess solvent, coating the surface homogeneously, and drying the solvent by evaporation from the substrate surface. Finally, the rectifier Al contacts with a diameter of 1 mm (7.85×10^{-3} cm^2) and a thickness of about 1000–1500 Å on the front face of the semiconductor were formed in the same system. The measurements of capacitance and conductance were performed at room temperature using HP41912-A-LF impedance analyzer at room temperature. Both the schematic diagram of the Al/(BSA-doped-PANI)/p-InP structures and measured impedance measurements system are given in Fig. 1.

3 Result and discussions

Figures 2, 3, 4 and 5 presents the characteristics of C and G/ω versus voltage for Al/BSA-doped-PANI/p-InP structure between 1 and 200 kHz, respectively. Three voltage interval regions as inversion (− 3/0 V), depletion (0/2 V) and accumulation (2/5 V) can easily be seen from C–V plot in Fig. 2. Figure 2 confirmed the MIS behavior of the structure and can also be interpreted in five regions adding with strong and weak inversion and accumulation regions [33]. The values of C are almost independent from applied biases in strong accumulation and inversion regions while it variates with voltage in the weak parts of these regions. On the other hand, it is clearly seen that C is strongly dependent in voltages in the
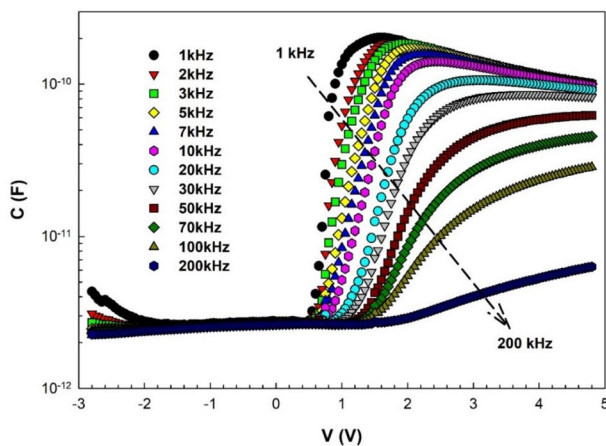

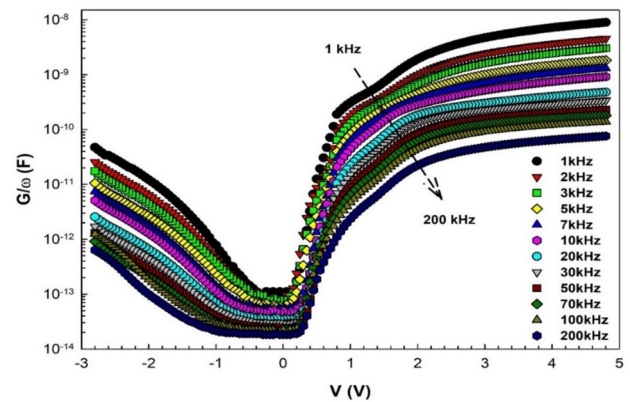**Fig. 3** The structure's G/ω–V graph at 1–200 kHz interval
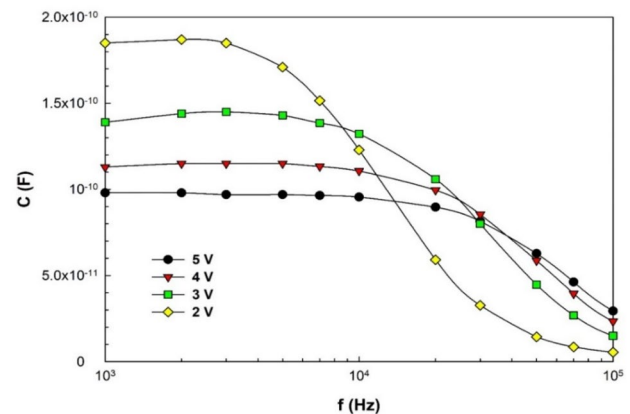
Fig. 4 The dependency of frequency to the capacitance for structure

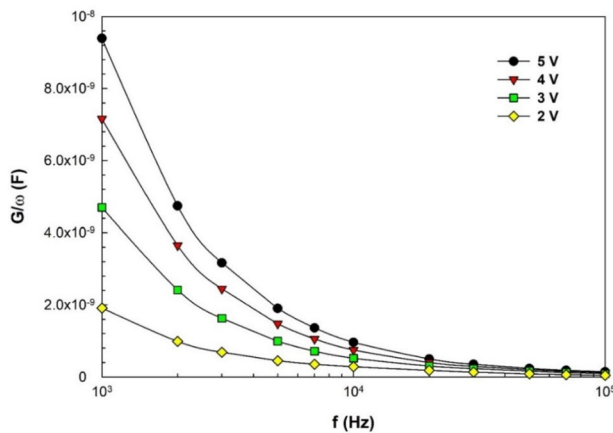**Fig. 2** The structure's C–V graph at 1–200 kHz interval

Fig. 5 The dependency of frequency to the conductance for structure

depletion region. Generally, in the ideal case, the changes in C seem like S shape, but a peak is observed in the accumulation region due to the presence of the series resistance (R_s) and the interlayer. Moreover, at very high frequencies, the C and G/ω values are independent from frequency and increase with increasing voltages in MPS structures. The existence of surface states (N_{ss}) and polarization causes a scattering at C and G/ω values for lower frequencies in the depletion region as seen in Figs. 2 and 3. Since it is not possible for N_{ss} to follow the AC signal at high frequencies, contrary to low frequencies, there is no contribution of N_{ss} to the calculation of C and G values. As presented in Fig. 2, the C values at forward biases are almost similar between 1 and 10 kHz and after this decreased with increasing frequencies. Besides, C values are not dependent in voltages at higher frequencies as the effect of N_{ss} at these frequencies is considered. G values for the specific voltages of the forward biases decrease exponentially with the frequency increment as indicated in Fig. 3. In general, these changes in the C and G especially at low frequencies are the results of dipole and surface polarization under external electric field and the existence of surface states that relocates the charges from their equilibrium position or traps. MS structure with an interfacial layer has also some advantages compared to MS structure because of it can prevent an interface-diffusion and reaction between metal and semiconductor and deactivates many surface states.

In Figs. 4 and 5, frequency-dependent C and G values between 2 and 5 V interval which are sufficient forward biases, were illustrated. Figure 4 presents that the capacitance in this voltage interval decreases with frequency increment. Consequently, it appears that the C values are not dependent on the biases at a sufficiently high frequency of 200 kHz. The contribution of N_{ss} to capacitance can be ignored at high frequencies as it was too low to take into account. Figure 5 indicates that the conductance at

the same voltage interval are reduced exponentially with increasing frequencies.

Utilizing from the acquired C and G data at room temperature, the dielectric specifications of the BSA doped interlayered structure were investigated for different frequency levels. Thus, the following expressions were used to specify the values of ε′, ε″, tanδ and $σ_{ac}$ for the interlayer, respectively [34, 35].

$$\varepsilon' = \frac{Cd}{\varepsilon_o A} \tag{1}$$

$$\varepsilon'' = \frac{Gd}{\varepsilon_o \omega A} \tag{2}$$

$$\tan \delta = \frac{\varepsilon''}{\varepsilon'} \tag{3}$$

$$\sigma_{ac} = \varepsilon'' \omega \varepsilon_o \tag{4}$$

where free space charge is $ε_o$ and equals to 8.85×10^{-14} F/cm. The interlayer thickness is d and the rectifier contact area is A in cm^{-2}. As can be seen in Eq. (3), the loss tangent/dissipation factor (tan δ) is the ratio of dielectric loss (ε″) to dielectric constant (ε′) of the material and also it measures the ratio of the electric energy lost to the energy stored in an applied electric field.

Usually the complex electric modulus (M^*) formalisms are used to explain the dielectric relaxation of the interfacial layer materials and it is extracted from the complex dielectric permittivity (ε* = 1/M*) data using the following equation [35]:

$$M^* = \frac{1}{\varepsilon^*} = M' + jM\varepsilon'' = \frac{\varepsilon'}{\varepsilon'^2 + \varepsilon\varepsilon''^2} + j\frac{\varepsilon\varepsilon''}{\varepsilon'^2 + \varepsilon''^2} \tag{5}$$

As a function of applied biases, the values of the real and imaginary parts of complex dielectric constant (ε′, ε″) and electric modulus (M′ and M″), and ac electrical conductivity ($σ_{ac}$) were extracted from Figs. 2 and 4. The figures of the ε′, ε″ and tanδ versus voltage are indicated in Figs. 6, 7 and 8, respectively.

Contrary to the inversion region, ε′ and ε″ are strongly dependent on frequencies and applied biases in the accumulation and depletion regions. An explicit peak seen in the depletion region in Fig. 6 and this peak is conceivably occurred when hopping frequencies of the carriers is almost equal to the external applied field. This indicates a strong relation between dielectric characteristics and conduction mechanisms of the structure.

At lower frequencies, similarly in Figs. 9, 10 and 11 the values of ε′, ε″ and tanδ exponentially decrease with frequency increment. As from these results, the external electric field application (V = E × d) that removes the
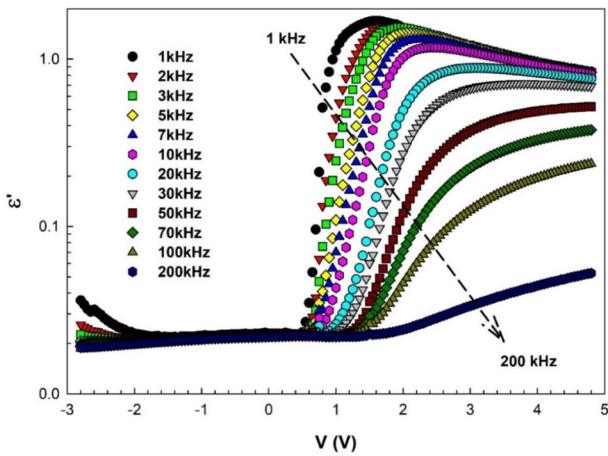
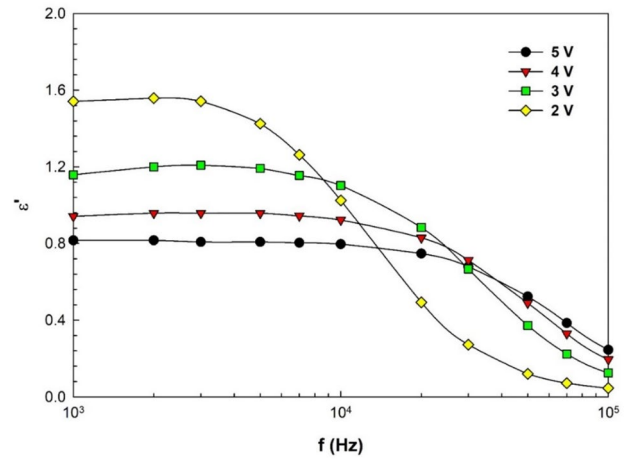**Fig. 6** The structure's ε′–V graph at 1–200 kHz interval
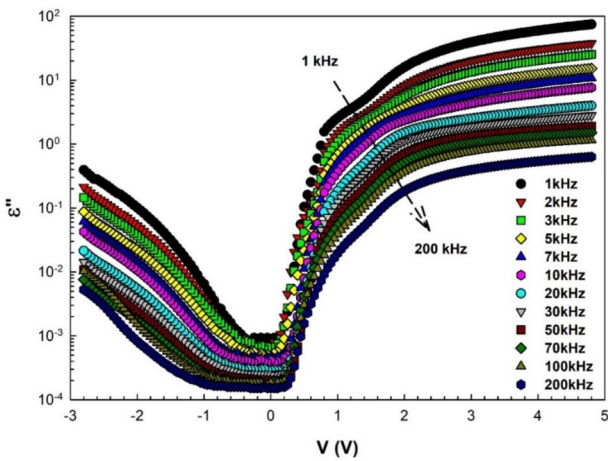

Fig. 9 The structure's ε′–f graph at several biases

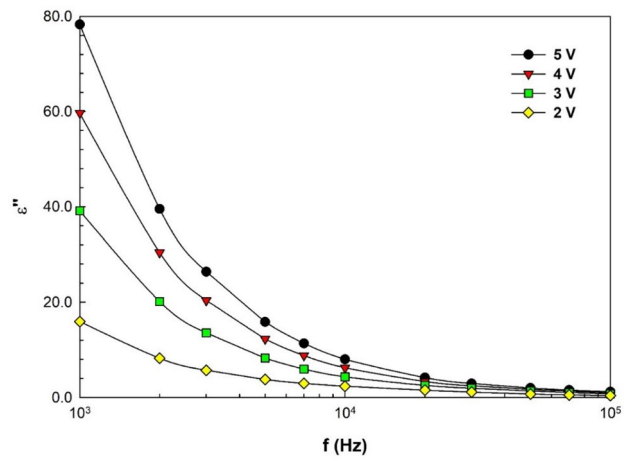**Fig. 7** The structure's ε″–V graph at 1–200 kHz interval
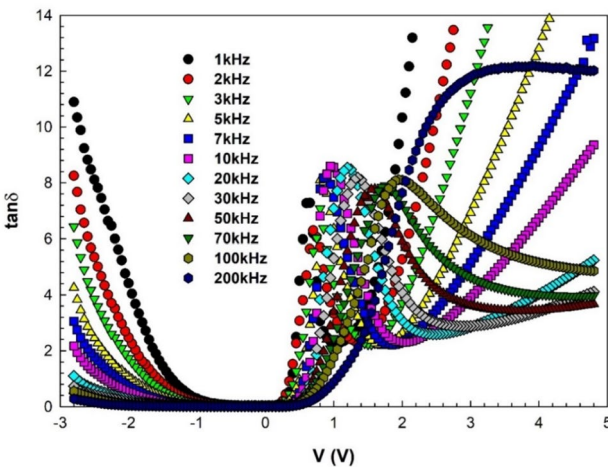

Fig. 10 The structure's ε″–f graph at several biases

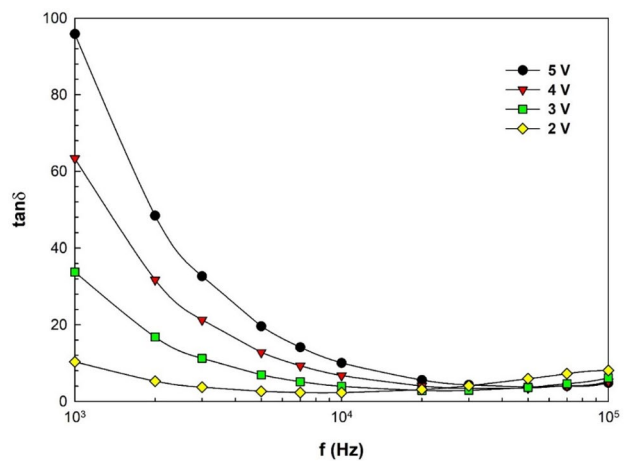**Fig. 8** The structure's tanδ–V graph at 1–200 kHz interval

Fig. 11 The structure's tanδ–f graph at several biases

carriers from equilibrium position is able to polarize the dielectric material.

Eventually, the decreases in the values of the ε', ε'', and tanδ by frequency increment can be elucidated by the interface polarization mechanism. The interface state charges at low frequencies can contribute to the C and G values and hence to the complex dielectric values as they can easily track the alternative current signal. Noticeably in narrow-bandgap semiconductor, the charges have not adequately freed to proceed so that they may be easy treed and so lead to increase of the polarization [36, 37]. Contrary, the decrement in ε', ε'' and tanδ with frequency increase can be explained by many dipoles that have not enough time to orient themselves in the ac electric field direction [38].

Several researches have been made on the electric modulus (M*) in terms of polarization conduction mechanisms [39–42]. Electric modulus formalism is their way of defining the dielectric features of the devices. Hence, the M′–V and M″–V plots of the MS structure with BSA doped PANI interlayer were presented in Figs. 12 and 13, respectively. M′/M″–V plots, presented in Figs. 12 and 13, show two specific peaks at the inverse region by the reason of surface states density distribution at BSA doped-PANI/semiconductor interface [43, 44]. It is observed that the M values increase with increasing frequencies in the reverse biased region while the opposite situation is observed in the forward biased region. As a result, after the increase in the reverse polarization, the values of M formed a peak around zero volts for all frequencies in the transition to the positive voltages, and then converged to zero with the voltage increase. The variations indicated in Figs. 12 and 13 for M′ and M″ can be ascribed by the sensibility of the dielectric relaxation mechanisms to frequency and biases of the inversion charges.
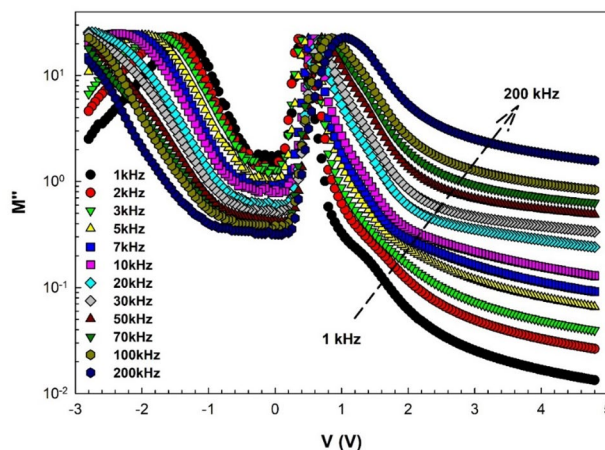

Fig. 13 The structure's M″–V graph at 1–200 kHz interval

Besides, the frequency dependent of M′ and M″ at several biases were also presented in Figs. 14 and 15. The M′ and M″ values increase with increasing frequency.

The ac electrical conductivity σ_{ac} for various frequencies was given in Fig. 16. The σ_{ac} value decreases by frequencies. In addition, the electrical conductivity increases with increasing applied biases in Fig. 17. Generally, this higher σ_{ac} values solely contribute to the dielectrics losses and are not important at higher frequency levels as it merges to infinity at zero frequency. As can be seen from Fig. 17 (σ vs lnf plots), for accumulation region or sufficiently high forward bias voltages the value of conductivity becomes almost constant at low and intermediate frequencies which is compatible with the dc conductivity (σ_{dc}), but the high frequency dispersion phenomena in conductivity is compatible with the ac conductivity (σ_{ac}).
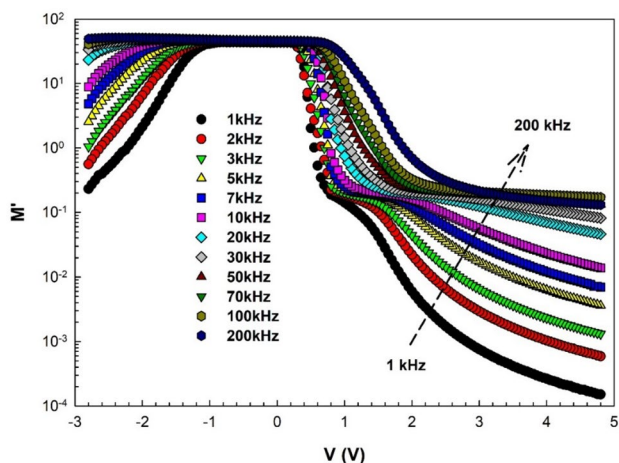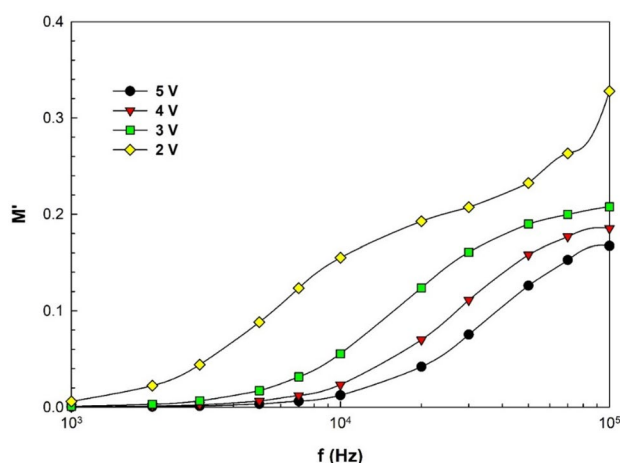

Fig. 12 The structure's M′–V graph at 1–200 kHz interval

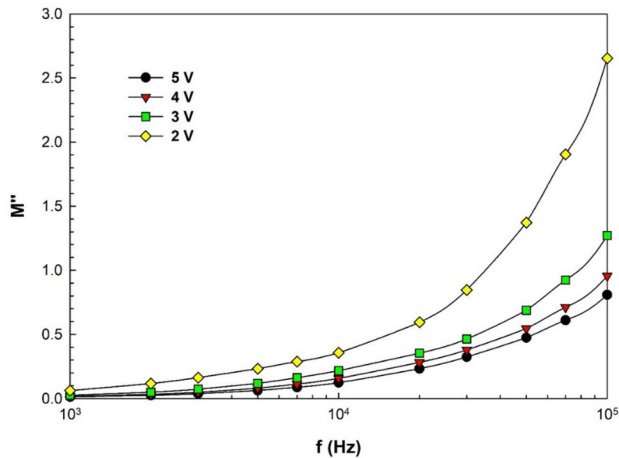**Fig. 14** The structure's M′–f graph at several biases

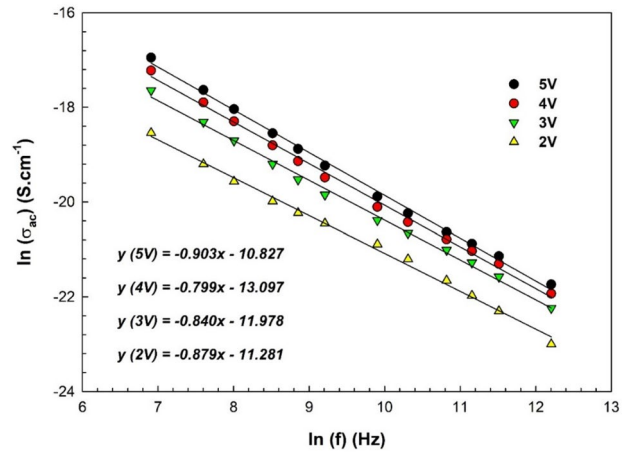**Fig. 15** The structure's M″–f graph at several biases

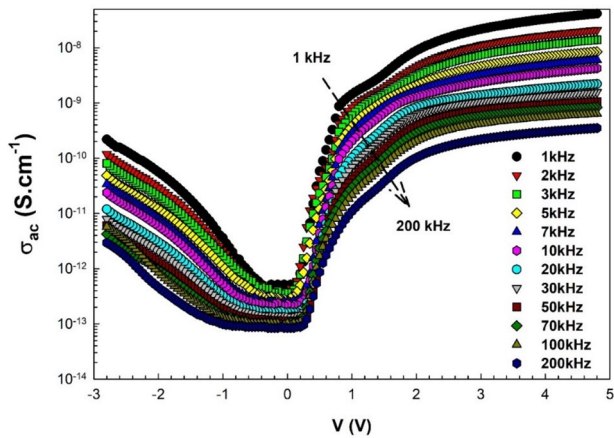**Fig. 18** The structure's ln σ$_{ac}$–ln f graph at several biases

Fig. 16 The structure's σ$_{ac}$–V graph at 1–200 kHz interval
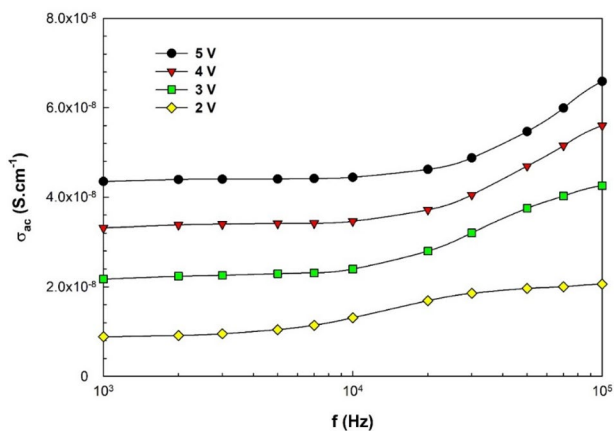

Fig. 17 The structure's σ$_{ac}$–f graph at several biases

The expression for σ$_{ac}$ in terms of angular frequency (ω) can be derived as [45]. Traditionally, the carriers jump from traps to other located in the semiconductor's bandgap causes an increase in σ$_{ac}$ and derived as in the following equation [45].

$$\sigma_{ac} = A\omega^s \tag{6}$$

As for the achieved experimental data, it is clear that conduction mechanisms of the structure are extremely depend on frequency, polarization, interlayer homogeneities and semiconductor's doping concentrations. In Eq. (6), the frequency exponent s measures the level of contact of the charge carriers with the lattice [46]. As can be seen from Fig. 18, the frequency exponent s which is obtained from the slope of the double logarithmic σ$_{ac}$ versus ω plot changes between 0.840 and 0.903 implied that the existence relaxation and polarization phenome.

After all, the alteration in dielectric parameters are the consequence of relaxation phenomena and the surface states existence and their relaxation time. On the other hand, these changes at enough high frequencies are the result of the series resistance only at accumulation region. The decrease in C and increase in G at accumulation region is the result of inductive behavior of the structure. In summary, both the electric and dielectric properties especially depend on interfacial insulator/polymer layer, its thickness and homogeneity, polarization processes, surface states and their relaxation times, frequency, and applied bias voltage or electric field [47, 48].

4 Conclusions

The admittance spectroscopy data (C–V and G/ω–V) of the BSA doped PANI interlayered MS structures have been examined between 1 and 200 kHz intervals. The ε′, ε″, M′, M″, and σ$_{ac}$ values were acquired as functions of frequencies

and applied biases. Experimental data were validated that the dispersion in ε', ε'', tanδ, M', M'' and σ_{ac} values are notably high particularly at lower frequency levels due to the oriental and the interfacial polarizations, as well as the surface states (N_{ss}) and the BSA doped-PANI interlayer. Such behavior in ε', ε'', and tanδ, behavior with frequency was also explained by Maxwell–Wagner relaxation. Accordingly, the polymeric material can be handily polarized at lower and intermediate frequencies under an external bias which dislocates the charges from their equilibrium position. ε'–f and ε''–f plots at several forward biases were examined to view the biases effect on the dielectric properties. As for the relaxation processes, M' values attain a maximum value at higher frequencies for each bias ($M_\infty = 1/\varepsilon_\infty$). The σ versus logf plot for sufficiently high voltages exhibited both low and high frequency dispersion phenomena such that at low frequencies σ value corresponding to the dc conductivity (σ_{dc}), but at high frequencies it corresponds to the ac conductivity (σ_{ac}).

References

1. S.O. Tan, Comparison of graphene and zinc dopant materials for organic polymer interfacial layer between metal semiconductor structure. IEEE Trans. Electron Devices **64**(12), 5121–5127 (2017)

2. Ş. Altındal, H. Uslu, The origin of anomalous peak and negative capacitance in the forward bias capacitance-voltage characteristics of Au/PVA/n-Si structures. J. Appl. Phys. **109**(7), 074503 (2011)

3. S.A. Yerişkin, M. Balbaşı, I. Orak, The effects of (graphene doped-PVA) interlayer on the determinative electrical parameters of the Au/n-Si (MS) structures at room temperature. J. Mater. Sci. **28**(18), 14040–14048 (2017)

4. H. Tecimer, S.O. Tan, Ş. Altındal, Frequency-dependent admittance analysis of the metal-semiconductor structure with an interlayer of Zn-doped organic polymer nanocomposites. IEEE Trans. Electron Devices **65**(1), 231–236 (2017)

5. H. Tecimer, On the frequency–voltage dependent electrical and dielectric profiles of the Al/(Zn-PVA)/p-Si structures. J. Mater. Sci. **29**(23), 20141–20145 (2018)

6. G.E. Demir, İ. Yücedağ, Y. Azizian-Kalandaragh, Ş. Altındal, Temperature and interfacial layer effects on the electrical and dielectric properties of Al/(CdS-PVA)/p-Si (MPS) structures. J. Electron. Mater. **47**(11), 6600–6606 (2018)

7. H.C. Card, E.H. Rhoderick, Studies of tunnel MOS diodes I. Interface effects in silicon Schottky diodes. J. Phys. D **4**(10), 1589 (1971)

8. C.C. Lin, Y.H. Wu, T.H. Hung, Y.T. Chang, Impact of interfacial layer position on resistive switching behaviors for ZrTiO x-based metal–insulator–metal devices. IEEE Trans. Nanotechnol. **13**(4), 634–638 (2014)

9. S.O. Tan, H. Tecimer, O. Çiçek, Comparative investigation on the effects of organic and inorganic interlayers in Au/n-GaAs Schottky diodes. IEEE Trans. Electron Devices **64**(3), 984–990 (2017)

10. N.G. McCrum, B.E. Read, G. Williams, *Anelastic and dielectric effects in polymeric solids* (Wiley, New York, 1967)

11. E. Mar et al., Evaluation of electric and dielectric properties of metal–semiconductor structures with 2% GC-doped-($Ca_3Co_4Ga_{0.001}O_x$) interlayer. IEEE Trans. Electron Devices **65**(9), 3901–3908 (2018)

12. M.M. Hoque et al., The impedance spectroscopic study and dielectric relaxation in A ($Ni_{1/3}Ta_{2/3}$) O_3 [A = Ba, Ca and Sr]. Phys. B **407**(18), 3740–3748 (2012)

13. S. Yasufuku et al., Maxwell-wagner dielectric polarization in polypropylene film/aromatic dielectric fluid system for high voltage capacitor use. IEEE Trans. Electr. Insul. **6**, 334–342 (1979)

14. J. Chen et al., Current–voltage–temperature and capacitance–voltage–temperature characteristics of TiW alloy/p-InP Schottky barrier diode. J. Alloys Compd. **649**, 1220–1225 (2015)

15. B. Akkal et al., Illumination dependence of I-V and C–V characterization of Au/InSb/InP (1 0 0) Schottky structure. Appl. Surf. Sci. **253**(3), 1065–1070 (2006)

16. V. Janardhanam et al., Temperature dependency and carrier transport mechanisms of Ti/p-type InP Schottky rectifiers. J. Alloys Compd. **504**(1), 146–150 (2010)

17. P.S. Reddy, V. Janardhanam, I. Jyothi, S.H. Yuk, V.R. Reddy, J.C. Jeong, S.N. Lee, C.J. Choi, Modification of Schottky barrier properties of Ti/p-type InP Schottky diode by polyaniline (PANI) organic interlayer. J. Semicond. Technol. Sci. **16**(5), 664–674 (2016)

18. O. Çiçek, S.O. Tan, H. Tecimer, Ş. Altındal, Role of graphene-doped organic/polymer nanocomposites on the electronic properties of Schottky junction structures for photocell applications. J. Electron. Mater. **47**(12), 7134–7142 (2018)

19. H.U. Tecimer, M.A. Alper, H. Tecimer, S.O. Tan, Ş. Altındal, Integration of Zn-doped organic polymer nanocomposites between metal semiconductor structure to reveal the electrical qualifications of the diodes. Polym. Bull. **75**(9), 4257–4271 (2018)

20. Y.S. Altındal, M. Balbaşı, A. Tataroğlu, Frequency and voltage dependence of dielectric properties, complex electric modulus, and electrical conductivity in Au/7% graphene doped-PVA/n-Si (MPS) structures. J. Appl. Polym. Sci. (2016). https://doi.org/10.1002/app.43827

21. J. Jang, J. Ha, J. Cho, Fabrication of water-dispersible polyaniline-poly (4-styrenesulfonate) nanoparticles for inkjet-printed chemical-sensor applications. Adv. Mater. **19**(13), 1772–1775 (2007)

22. S. Ashokan, V. Ponnuswamy, P. Jayamurugan, Comparative study of pure polyaniline with various oxidants by a template free method. Mater. Sci. Semicond. Process. **30**, 494–501 (2015)

23. J. Stejskal et al., The effect of polymerization temperature on molecular weight, crystallinity, and electrical conductivity of polyaniline. Synth. Met. **96**(1), 55–61 (1998)

24. P.J. Saikia, P.C. Sarmah, Investigation of polyaniline thin film and schottky junction with aluminium for electrical and optical characterization. Mater. Sci. Appl. **2**(08), 1022 (2011)

25. S. Ashokan et al., Influence of the counter ion on the properties of organic and inorganic acid doped polyaniline and their Schottky diodes. Superlattices Microstruct. **85**, 282–293 (2015)

26. Z. Zhang, Z. Wei, M. Wan, Nanostructures of polyaniline doped with inorganic acids. Macromolecules **35**(15), 5937–5942 (2002)

27. G. Ćirić-Marjanović, Recent advances in polyaniline research: polymerization mechanisms, structural aspects, properties and applications. Synth. Met. **177**, 1–47 (2013)

28. J. Stejskal et al., Polyaniline prepared in the presence of various acids: a conductivity study. Polym. Int. **53**(3), 294–300 (2004)

29. S.H. Kim, J.H. Seong, K.W. Oh, Effect of dopant mixture on the conductivity and thermal stability of polyaniline/Nomex conductive fabric. J. Appl. Polym. Sci. **83**(10), 2245–2254 (2002)

30. B. Belaabed, S. Lamouri, J.L. Wojkiewicz, Curing kinetics, thermomechanical and microwave behaviors of PANI-doped BSA/epoxy resin composites. Polym. J. **43**(8), 683 (2011)

31. W.H. Jang et al., Synthesis and electrorheology of camphorsulfonic acid doped polyaniline suspensions. Colloid Polym. Sci. **279**(8), 823–827 (2001)

32. W. Yin, E. Ruckenstein, Soluble polyaniline co-doped with dodecyl benzene sulfonic acid and hydrochloric acid. Synth. Met. **108**(1), 39–46 (2000)

33. A. Kaya et al., The investigation of dielectric properties and ac conductivity of Au/GO-doped PrBaCoO nanoceramic/n-Si capacitors using impedance spectroscopy method. Ceram. Int. **42**(2), 3322–3329 (2016)

34. E.H. Nicollian, J.R. Brews, E.H. Nicollian, *MOS (metal oxide semiconductor) physics and technology*, vol. 1987 (Wiley, New York et al., 1982)

35. S.K. Tripathi, M. Sharma, Analysis of the forward and reverse bias IV and CV characteristics on Al/PVA: n-PbSe polymer nanocomposites Schottky diode. J. Appl. Phys. **111**(7), 074513 (2012)

36. J. Ho, T.R. Jow, S. Boggs, Historical introduction to capacitor technology. IEEE Electr. Insul. Mag. **26**(1), 20–25 (2010)

37. J.-H. Lin, J.-J. Zeng, Y.-J. Lin, Electronic transport for graphene/n-type Si Schottky diodes with and without H_2O_2 treatment. Thin Solid Films **550**, 582–586 (2014)

38. A. Chełkowski, *Dielectric physics*, vol. 9 (Elsevier, Amsterdam, 1980)

39. A. Dutta, C. Bharti, T.P. Sinha, AC conductivity and dielectric relaxation in $CaMg_{1/3}Nb_{2/3}O_3$. Mater. Res. Bull. **43**(5), 1246–1254 (2008)

40. M.M. Hoque et al., Dielectric relaxation and conductivity of $Ba(Mg_{1/3}Ta_{2/3})O_3$ and $Ba(Zn_{1/3}Ta_{2/3})O_3$. J. Mater. Sci. Technol. **30**(4), 311–320 (2014)

41. S. Alptekin, A. Tataroğlu, Ş. Altındal, Dielectric, modulus and conductivity studies of Au/PVP/n-Si (MPS) structure in the wide range of frequency and voltage at room temperature. J. Mater. Sci. **30**, 6853–6859 (2019)

42. S. Demirezen, E.E. Tanrıkulu, Ş. Altındal, The study on negative dielectric properties of Al/PVA (Zn-doped)/p-Si (MPS) capacitors. Indian J. Phys. **93**, 739–747 (2019)

43. S.O. Tan et al., Electrical characterizations of Au/ZnO/n-GaAs Schottky diodes under distinct illumination intensities. J. Mater. Sci. **27**(8), 8340–8347 (2016)

44. M. Gökçen et al., UV illumination effects on electrical characteristics of metal–polymer–semiconductor diodes fabricated with new poly (propylene glycol)-b-polystyrene block copolymer. Compos. B Eng. **57**, 8–12 (2014)

45. A. Lösche, N.F. Mott, E.A. Davis, Electronic processes in noncrystalline materials clarendon-press, Oxford 1971 437 Seiten.£ 7, 50. Kristall Tech. **7**(4), K55–K56 (1972)

46. S. Amrin, V.D. Deshpande, Dielectric relaxation and ac conductivity behavior of carboxyl functionalized multiwalled carbon nanotubes/poly (vinyl alcohol) composites. Physica E **87**, 317–326 (2017)

47. X. Wu, E.S. Yang, H.L. Evans, Negative capacitance at metal-semiconductor interfaces. J. Appl. Phys. **68**(6), 2845–2848 (1990)

48. H.N. Chandrakala, B. Ramaraj, G.M. Madhu, The influence of zinc oxide–cerium oxide nanoparticles on the structural characteristics and electrical properties of polyvinyl alcohol films. J. Mater. Sci. **47**(23), 8076–8084 (2012)